Changes in the mean-square charge radii and magnetic moments of neutron-deficient Tl isotopes

A. E. Barzakh,* L. Kh. Batist, D. V. Fedorov, V. S. Ivanov, K. A. Mezilev, P. L. Molkanov, F. V. Moroz, S. Yu. Orlov, V. N. Panteleev, and Yu. M. Volkov

Petersburg Nuclear Physics Institute (PNPI), NRC Kurchatov Institute, Gatchina 188300, Russia

(Received 14 June 2013; revised manuscript received 21 July 2013; published 19 August 2013)

In-source laser spectroscopy experiments for neutron-deficient thallium isotopes at the 276.9-nm atomic transition have been carried out at the Investigation of Radioactive Isotopes on Synchrocyclotron facility of Petersburg Nuclear Physics Institute. New data on isotope shifts and the hyperfine structure for $^{183-207}$Tl isotopes and isomers are presented. The changes in the mean-square charge radii and magnetic-moment values are deduced. It is shown that nuclear properties of Tl isotopes and isomers smoothly change at the neutron midshell and beyond without development of strong deformation in contrast to the adjacent Hg nuclei. A rather great isomer shift between $I = 1/2$ and $I = 9/2$ states for odd Tl isotopes is preserved for both sides of the previously investigated mass range. For the first time, a similar isomer shift is found for the odd-odd isotope ^{186}Tl. The close resemblance of the charge radii isotopic behavior for the Tl and Pb ground states is demonstrated.

DOI: 10.1103/PhysRevC.88.024315 PACS number(s): 21.10.Ft, 21.10.Ky, 27.80.+w, 31.30.Gs

I. INTRODUCTION

As stressed in a recent review [1], understanding the occurrence of shape coexistence in atomic nuclei is one of the greatest challenges faced by theories of nuclear structure. In this respect, the neutron-deficient isotopes near $Z = 82$ exhibit the most extensive manifestation of shape coexistence. In these nuclei, examples of prolate, oblate, and spherical structures have been found at low excitation energy (see Ref. [1] and references therein). Although the shape coexistence is a common feature of the all isotopic chains in this region (in the vicinity of the neutron midshell $N = 104$), the behavior of the ground- and isomeric state shapes differs markedly for different Z's. In the Hg isotopic chain ($Z = 80$), strong odd-even staggering is observed (the ground states of the odd-A isotopes with $N < 105$ are strongly deformed, whereas, the even-A isotopes remain nearly spherical or weakly deformed, see Ref. [2]). Both odd- and even-neutron Au isotopes ($Z = 79$) change their shapes from weakly oblate (or triaxial) to strongly prolate deformed after $N = 107$ due to the influence of the $\pi h_{9/2}$ intruder orbital [3]. At the same time, the neutron-deficient even-A and odd-A Pb nuclei ($Z = 82$) remain essentially spherical up to and beyond the neutron midshell at $N = 104$ [4].

The investigations of the neutron-deficient Tl isotopes ($Z = 81$) play an important role in the understanding of shape coexistence phenomena in this region of the nuclide chart. These isotopes reveal, along with the near-spherical ground states, the presence of oblate structures that result from the occupancy of $\pi h_{9/2}$ and $\pi h_{11/2}$ orbitals as well as prolate configurations that involve $\pi h_{9/2}$, $\pi i_{13/2}$, and $\pi f_{7/2}$ orbitals (e.g., see Refs. [5,6]).

Observables that give model-independent information on the ground- and isomeric state shapes are charge radius changes determined by atomic spectroscopy. So far, atomic spectroscopy measurements for a restricted set of thallium isotopes $^{186-205,207,208}$Tl [7–18] have been performed. Isotope shifts (ISs) and hyperfine structures (hfs) were measured in the 535-nm transition. Thus, the previous laser spectroscopic investigations ended at $N = 105$ before the neutron midshell where the most pronounced shape staggering or shape transition effects are expected. It is of importance to continue these studies beyond the midshell.

Previously, it was also found that some Tl isomers with $I = 9/2$ (^{187,191,193}Tl^m) have markedly greater deformation than the corresponding ground states (see Ref. [15] and references therein). In particular, this reveals itself in a rather great isomer shift in the optical lines. The isomers with $I = 9/2$ are well known for the majority of the odd neutron-deficient Tl nuclei ($A = 181$–201; see Ref. [19]). All of them are treated as intruder states with the odd proton in the $\pi h_{9/2}$ shell at the moderate oblate deformation. This interpretation is supported by the observation of the strongly coupled bands built on these states (see Ref. [1] and references therein). Intruder-based states with the ($\pi h_{9/2}$,$\nu i_{13/2}$) configuration were also found in odd-odd Tl nuclei [20–22]. The lowest member of the corresponding multiplet becomes a comparatively long-lived isomer in some cases ($I = 8$ for ^{192}Tl, $I = 9$ for ^{188}Tl, and $I = 10$ for ^{186,184}Tl). It is of importance to continue the laser spectroscopic study of the Tl isotopic chain to check whether the great isomer shift (i.e., the marked difference between the ground- and isomeric state deformations) preserves for the lighter ($A < 187$) and heavier ($A > 193$) odd Tl isotopes and whether it exists for intruder-based states in odd-odd Tl isotopes as well.

The method of resonance laser ionization in the laser ion source for the thallium isotope shift and hyperfine structure measurements has been chosen as the most efficient tool for short-lived isotope production and investigation [23–25]. All measurements were carried out at the laser-nuclear complex [26] of the Investigation of Radioactive Isotopes on Synchrocyclotron (IRIS) facility, working online with the 1-GeV proton beam of the Petersburg Nuclear Physics Institute (PNPI) synchrocyclotron.

*Corresponding author: barzakh@mail.ru

II. EXPERIMENTAL SETUP

The laser system designed by Medical Sterilization Systems Company (Moscow region, Russia) consists of copper vapor lasers (CVLs), dye lasers, nonlinear crystals, and optical elements for manipulating laser beams. The CVL system, which consists of a laser oscillator and two parallel amplifiers, is built by using commercially produced sealed-off discharge-heated CVL tubes LT-40Cu. The CVLs run at a pulse repetition rate of 11 kHz with a pulse duration of 20 ns. All three tubes are triggered simultaneously and provide two beams with an average power of 50 W. The CVL radiation is composed of two spectral lines of 511 and 578 nm.

The laser setup has been arranged to provide the two-step resonance ionization of Tl atoms,

$$6p\ ^2P_{1/2} \xrightarrow[\text{NBL}]{276.9\,\text{nm}} 6d\ ^2D_{3/2} \xrightarrow[\text{CVL}]{511+578\,\text{nm}} \text{continuum}.$$

The narrow-band scanning dye laser [(NBL); linewidth is about 700 MHz] on the first step was tuned to a 276.9-nm transition. As the second step, we used the beam of the CVL laser to ionize the thallium atom into continuum. With a laser dye solution (Rhodamine 110), a fundamental laser wavelength of 554 nm has been produced. Doubling this frequency with a nonlinear β-barium borate crystal, the necessary wavelength of 276.9 nm has been obtained. Tuning of the dye laser wavelength is provided by rotation of the etalon and diffraction grating in the dye laser cavity. An electromechanical system for the laser frequency scanning has been used. This system incorporates step motors for the setting of the narrow-band laser etalon and diffraction grating positions, a frequency readout that uses the wave meter (model LM-007) and communication to the data-acquisition system. Such a system provides the smooth narrow-band scanning by self-calibration of the etalon and grating positions according to the laser line quality criterion. (See detailed setup description in Ref. [26]).

Radioactive Tl isotopes under study were produced by 1-GeV protons of the PNPI synchrocyclotron in a high-density uranium monocarbide target [27] with a thickness of 91 g cm^{-2}.

The atoms are thermally released from the target to the ion source cavity (a tungsten tube with a length of 40 mm and 1.5 mm in diameter). Laser beams are introduced into the same cavity through the quartz window in the front-end back side to provide two-step resonance ionization of the atoms under investigation. The distance between the laser setup and the ion source is about 25 m. The wavelength of the narrow-band laser is scanned across the 276.9-nm transition. The photoion current at the collector of the mass separator increases at the resonance. Thus, the experimental spectra represent the dependence of the ion current on the scanned laser frequency. The detection of ion current is provided by α, β, or γ counting. Corresponding detectors are installed at the tape station.

III. EXPERIMENTAL RESULTS

In Fig. 1, some experimental hfs spectra of Tl isotopes are shown.

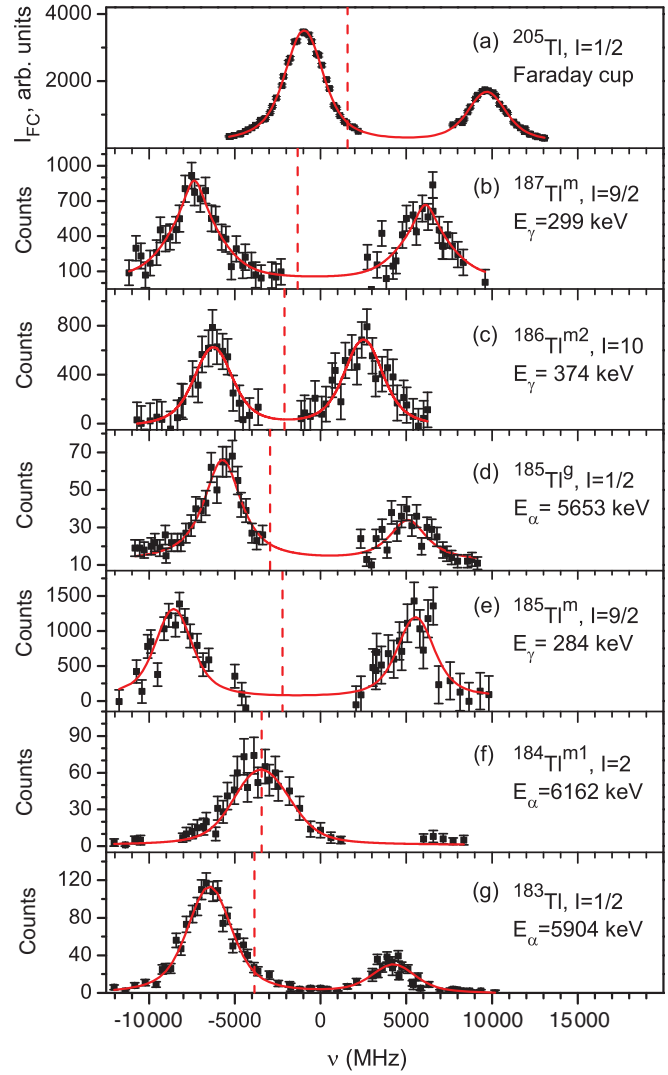

FIG. 1. (Color online) Hfs spectra of some Tl isotopes. In the insets, the atomic number, spin, and energies of the γ or α lines for ion current monitoring for the isotope in question are presented. Full lines are the results of the fitting with the Voigt profile. Vertical dashed lines mark the center of gravity of the corresponding hfs.

The position of the hyperfine components on the spectrum is determined by

$$\nu^{F,F'} = \nu_0 + \Delta\nu^{F'} - \Delta\nu^{F},$$

where ν_0 is the position of the center of gravity of the hyperfine structure, the prime symbol denotes the upper level of the transition, and

$$\Delta\nu^{F} = a\frac{K}{2} + b\frac{0.75K\,(K+1) - I\,(I+1)\,J\,(J+1)}{2\,(2I-I)\,(2J-1)\,I\,J}, \tag{1}$$

where $K = F(F+1) - I(I+1) - J(J+1)$, F is the total angular momentum of the atom ($F = |I-J|, |I-J|+1, \ldots, I+J$), and a and b are the magnetic dipole and electric quadrupole hyperfine coupling constants, respectively. These constants are proportional to the nuclear magnetic dipole (μ) and electric quadrupole (Q) moments, respectively.

Experimental data were fitted by the Voigt profile. In the fitting procedure, the ratio a'/a was fixed in accordance with its value for stable ^{205}Tl: $a(6d\ ^2D_{3/2},^{205}\mathrm{Tl})/a(6p\ ^2P_{1/2},^{205}\mathrm{Tl}) = -0.002\,013(19)$ [8,28]. Its change for the other isotopes due to hyperfine anomaly is less than 1%–3% (see Sec. V) and does not affect the results.

For the isotopes with $I > 1/2$, the quadrupole splitting of the upper level $6d\ ^2D_{3/2}$ of the scanned transition should be taken into account [constant b in Eq. (1)]. There are no experimental data concerned with the hfs quadrupole constant b for this level in the Tl atom. In the one-electron approximation [29],

$$a \sim \frac{\mu}{I}\left\langle\frac{1}{r^3}\right\rangle F_r(j, Z_i), \quad b \sim Q\left\langle\frac{1}{r^3}\right\rangle R_r\,(l, j, Z)\,,$$

where F_r and R_r are the relativistic corrections, $Z_i = Z - 11$, $l = 2$, and $j = 3/2$ for the d electron, and proportionality coefficients do not depend on Z or n (principal quantum number) [29]. Therefore, one can expect that the ratio,

$$P \equiv \frac{b}{Q}\frac{\mu}{aI}\frac{F_r}{R_r}$$

depends on the electronic configuration only and remains constant for all Tl homologs. Corresponding a and b constants were measured for $nd\ ^2D_{3/2}$ states ($n = 3$–5) of the homologs of Tl, namely, for Al [30], Ga [31], and In [32]. Values of Q and μ for ^{27}Al, ^{69}Ga, and ^{115}In were taken from Ref. [33]. The calculation shows that the assumption of the constancy of P for $nd\ ^2D_{3/2}$ states in the Tl homologs is justified in the limits of errors: $P(^{27}\mathrm{Al}) = -1.89(0.84)$, $P(^{69}\mathrm{Ga}) = -0.97(0.88)$, and $P(^{115}\mathrm{In}) = -0.81(0.23)$. The weighted mean value $P_{\mathrm{mean}} = -0.89(0.22)$ was used for the estimation of the $b(6d\ ^2D_{3/2})$ constant for Tl isotopes with $I > 1/2$ by the relation,

$$b(6d\ ^2D_{3/2}) = P_{\mathrm{mean}}\,Q\frac{a(6d\ ^2D_{3/2})I}{\mu}\frac{R_r}{F_r}.$$

The estimated quadrupole constant $b(6d\ ^2D_{3/2})$ proved to be small in comparison with our experimental uncertainties. For example, $b(6d\ ^2D_{3/2},^{193}\mathrm{Tl}^m) = 33(9)$ MHz; this corresponds to the maximal shift in the hfs sublevel of 14 MHz [see Eq. (1)]. The constant b was varied during the fitting in the limits of its error.

For isotopes with $I = 2$ (except for ^{184}Tl), the hyperfine splitting is small (∼2 GHz) in comparison with the laser linewidth (Doppler width ∼1.5 GHz and Lorenz width ∼2 GHz after frequency doubling), and a factors cannot be obtained by fitting. For ^{194}Tl, the constant $a(7s\ ^2S_{1/2})$ was fixed in accordance with its experimental value from Ref. [34]. Ratio

$$\rho^A(6p\ ^2P_{1/2}, 7s\ ^2S_{1/2}) = \frac{a^A(6p\ ^2P_{1/2})}{a^A(7s\ ^2S_{1/2})}$$

for Tl isotopes with $I = 2$ can be determined for $A = 196,194$ by using the experimental data from Refs. [7,34]: $\rho^{196}(6p\ ^2P_{1/2}, 7s\ ^2S_{1/2}) = 1.681(74)$, $\rho^{194}(6p\ ^2P_{1/2}, 7s\ ^2S_{1/2}) = 1.681(51)$. The weighted mean value,

$$\rho^{(I=2)}(6p\ ^2P_{1/2}, 7s\ ^2S_{1/2}) = 1.681\,(42)$$

was used to estimate the unknown $a^A(6p\ ^2P_{1/2})$ constants for $^{190,192}\mathrm{Tl}^g$ from the measured $a^A(7s\ ^2S_{1/2})$ constants in Ref. [7],

$$a^{A(I=2)}(6p\ ^2P_{1/2}) = \rho^{(I=2)}(6p\ ^2P_{1/2}, 7s\ ^2S_{1/2})a^{A(I=2)}(7s\ ^2S_{1/2}). \quad (2)$$

These values were fixed during the fitting procedure for these isotopes.

In Table I, isotope shifts for the 276.9-nm transition and a constants for the atomic ground state $6p\ ^2P_{1/2}$ in the Tl isotopic chain are presented. In column 4 along with the a constants obtained in the present paper, the a constants for $^{197,195,193,191,189,187}\mathrm{Tl}^m$ measured in our previous paper [35] as well as the a constants for ^{190,192}Tl recalculated by Eq. (2) are presented. For the light odd-odd Tl isotopes, the relative positions of the high ($I = 7$) and low ($I = 2$) spin states are unknown, and their designation as ground or isomeric states is based on the systematic ($188 < A < 196$; see Ref. [19]). For ^{186,184}Tl, the ordering of the lowest-lying 2^- and 7^+ states cannot be based on the systematic reliably and conditional designation as "$m1$" for the corresponding nuclei were used.

IV. CHANGES IN THE MEAN-SQUARE CHARGE RADII

The changes in the mean-square charge radii $\delta\langle r^2\rangle^{A,A'}$ are deduced from the measured isotope shift $\delta\nu^{A,A'}$ by the well-known relations [36],

$$\delta\nu^{A,A'} = F_\nu\lambda^{A,A'} + M_\nu\frac{A - A'}{AA'}, \quad (3)$$

where $M_\nu = M_\nu^{\mathrm{NMS}} + M_\nu^{\mathrm{SMS}}$, $M_\nu^{\mathrm{NMS}} = \frac{\nu}{(m_p/m_e)}$, $\lambda^{A,A'} = K(Z)\,\delta\langle r^2\rangle^{A,A'}$, ν is the transition frequency, M_ν^{NMS} and M_ν^{SMS} are the normal mass shift (NMS) and specific mass shift (SMS) constants, respectively, and $K(Z)$ takes the contribution of the higher-order radii moments in $\lambda^{A,A'}$ into account (see Refs. [36,37]).

The electronic factor F was calculated by Fricke [38] for different Tl atomic levels by single-configuration-Dirac-Fock (SCDF) *ab initio* calculations. From Table 5 in Ref. [8], one can easily calculate the needed F factors: $F_{535\,\mathrm{nm}} = -18.70$ and $F_{276.9\,\mathrm{nm}} = -12.66$ GHz fm^{-2}.

The value $F_{535\,\mathrm{nm}} = -18.94$ GHz fm^{-2} was used in Ref. [7] in accordance with calculations by SCDF [39]. Calculation by many-body perturbation theory gives $F_{535\,\mathrm{nm}} = -20.79$ GHz fm^{-2} [40]. A substantially different value of $F_{535\,\mathrm{nm}} = -15.65$ GHz fm^{-2} was obtained in the framework of the relativistic "coupled-cluster" approach [41].

The values $F_{535\,\mathrm{nm}} = -18.0$ GHz fm^{-2} and $M_{535\,\mathrm{nm}}^{\mathrm{SMS}} = 0$ were used in Ref. [36] in a combined analysis of the optical, the muonic atom, and the electron-scattering data in a model-independent way. The contribution of the higher-order radii moments was also determined in this analysis: $K(81) = 0.938$. These values of $F_{535\,\mathrm{nm}}$, $M_{535\,\mathrm{nm}}$, and $K(81)$ have been used in the present paper. The assumption of zero SMS is justified by

TABLE I. Isotope shifts for the 276.9-nm transition and magnetic hfs constants for the ground state $6p\ ^2P_{1/2}$ of Tl isotopes.

A	I	$\Delta\nu^{A,205}_{276.9\,\mathrm{nm}}$ (MHz)	$a^A(6p\ ^2P_{1/2})$(MHz)	$a^A(6p\ ^2P_{1/2})$(MHz), literature
207g	1/2	1030(240)	24 692(300)	
205g	1/2	0	21 272(100)	21 310.835(5)[a]
203g	1/2	−1070(150)[b]	21 160(120)	21 105.447(5)[a]
197m	9/2	−2790(250)	5900(77)[c]	
195m	9/2	−3330(110)	5634(55)[c]	
194m	7	−5450(130)	508(40)	
194g	2	−5530(220)		442(9)[d]
193m	9/2	−4350(140)	5583(34)[c]	
192m	7	−6660(330)	421(80)	
192g	2	−6500(390)	[630(19)][e]	
191m	9/2	−4930(120)	5506(32)[c]	
190m	7	−7380(180)	458(50)	
190g	2	−7040(270)	[802(23)][e]	
189m	9/2	−5660(150)	5474(56)[c]	
187m	9/2	−6330(300)	5389(43)[c]	
186$m1$	7	−9560(250)	420(60)	
186$m2$	10	−7350(220)	1670(40)	
185	1/2	−9500(400)	20 910(500)	
185m	9/2	−7480(280)	5470(300)	
184$m1$	2	−10 070(300)	1030(320)	
183g	1/2	−10 690(270)	21 060(480)	

[a]Reference [28].
[b]This value should be compared with the much more precise value from Ref. [8]: $\Delta\nu^{A,205}_{276.9} = -1038.5(0.1)$ MHz.
[c]Reference [35].
[d]Reference [34]. This value was fixed in the fitting procedure.
[e]This value has been calculated from $a^A(7s\ ^2S_{1/2})$ [7] by Eq. (2) and was fixed in the fitting procedure.

the estimation of SMS for some Tl levels in the framework of many-body perturbation theory [40].

The large overlap in the studied isotopes between the present data set and the previous studies using the 535-nm transition [7,10–18] allows the formalism of a King plot [36] to be used for determination of the F and M constants for the 276.9-nm transition by comparison of modified isotope shifts $\Delta\sigma_{A,A'}$ for the two transitions (see Fig. 2),

$$\Delta\sigma^{A,A'} = \Delta\nu^{A,A'}\frac{AA'}{(A-A')}.$$

According to Eq. (3), the plotted points (modified ISs) must lie on a straight line (the regression line),

$$\Delta\sigma^{A,A'}_{276\,\mathrm{nm}} = k\ \Delta\sigma^{A,A'}_{535\,\mathrm{nm}} + s.$$

The slope of the regression line is equal to the electronic factors ratio, and the intersection of the regression line with the y axis is equal to the linear combination of the mass shift constants for the transitions involved

$$s = M_{276\,\mathrm{nm}} - \frac{F_{276.9\,\mathrm{nm}}}{F_{535\,\mathrm{nm}}}M_{535\,\mathrm{nm}}.$$

With the assumption of zero SMS for the 535-nm transition, the King plot gives $k = F_{276.9\,\mathrm{nm}}/F_{535\,\mathrm{nm}} = 0.577(9)$ and $M_{276.9\,\mathrm{nm}} = 701(330)$ GHz amu. This means that $M^{\mathrm{SMS}}_{276.9\,\mathrm{nm}} = 0.2(6)M^{\mathrm{NMS}}_{276.9\,\mathrm{nm}}$. Note that SCDF calculations give $F_{276.9\,\mathrm{nm}}/F_{535\,\mathrm{nm}} = 0.677$ (see Ref. [8]).

In Table II, the values of $\delta\langle r^2\rangle$ for all investigated Tl isotopes and isomers are presented. All previously obtained IS data were reanalyzed with the unified electronic parameters set. Data for ^{187}Tl^g have not been included (the IS for this isotope was presented in a conference abstract [42] only). Scale uncertainty due to F and M indeterminacy may be estimated as

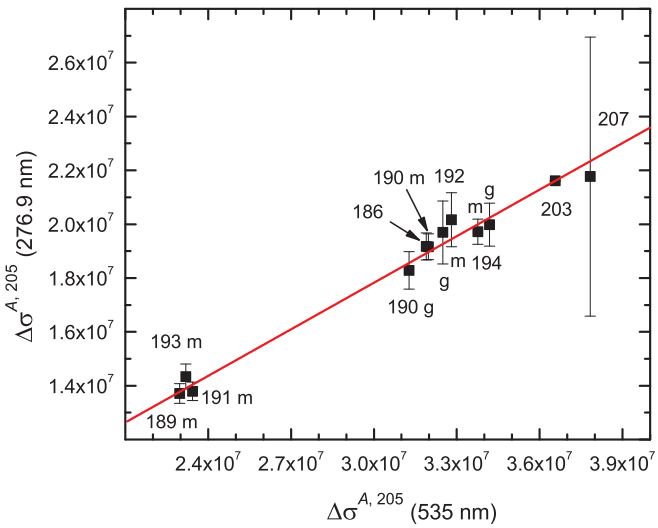

FIG. 2. (Color online) King plot for the 276.9-nm versus 535-nm transitions. Data for the 535-nm transition are taken from Refs. [7,10–18].

TABLE II. Deduced values of the mean-square charge radius changes for the Tl isotopic chains.

A	I	$\delta\langle r^2\rangle(\mathrm{fm}^2)$
208g	5	0.183(13){13}[a]
207g	1/2	0.1048(2){70}[b]
205g	1/2	0
204g	2	−0.0635(71){40}[c]
203g	1/2	−0.10321(2){700}[d]
202g	2	−0.1834(71){130}[c]
201g	1/2	−0.2077(9){150}[e]
200g	2	−0.2979(71){210}[c]
199g	1/2	−0.3116(71){220}[c]
198g	2	−0.4035(71){280}[f]
198m	7	−0.3804(71){270}[g]
197g	1/2	−0.4119(71){290}[f]
197m	9/2	−0.272(26){19}[h]
196g	2	−0.4795(5){340}[i]
196m	7	−0.4544(6){320}[i]
195g	1/2	−0.4820(71){340}[j]
195m	9/2	−0.324(11){23}[h]
194g	2	−0.5551(39){50}[i]
194m	7	−0.5481(5){380}[i]
193g	1/2	−0.5716(11){400}[e]
193m	9/2	−0.4111(10){290}[e]
192g	2	−0.6296(4){440}[i]
192m	7	−0.6358(6){450}[i]
191g	1/2	−0.6544(7){460}[i]
191m	9/2	−0.4899(6){340}[i]
190g	2	−0.7063(4){490}[i]
190m	7	−0.7223(5){510}[i]
189m	9/2	−0.5543(41){390}[e]
188m1	7	−0.8134(5){570}[i]
187m	9/2	−0.616(31){43}[h]
186m1	7	−0.9324(15){650}[k]
186m2	10	−0.719(23){50}[h]
185g	1/2	−0.938(41){66}[h]
185m	9/2	−0.731(29){51}[h]
184m1	2	−0.995(30){70}[h]
183g	1/2	−1.056(28){74}[h]

[a]IS data from Ref. [9] for the 378-nm transition were used. The electronic factor for this transition was calculated from the comparison of the field shifts for the pair $A = 203$, $A' = 205$ for 378- and 535-nm transitions with the assumption of $M_{\mathrm{SMS}} = 0$ for both transitions.
[b]IS data from Ref. [10].
[c]IS data from Ref. [11].
[d]IS data from Ref. [8].
[e]IS data from Ref. [14].
[f]IS data from Ref. [17].
[g]IS data from Ref. [16].
[h]Present paper.
[i]IS data from Ref. [7].
[j]IS data from Ref. [18].
[k]IS data from Ref. [13].

7% (see Ref. [43]). In Table II, the errors in parentheses reflect only the isotope shift uncertainties; the systematic errors that stem from the scaling uncertainty of the electronic factor and the specific mass shift are given in the curly brackets.

V. HYPERFINE STRUCTURE ANOMALY AND MAGNETIC MOMENTS

For evaluation of the magnetic moments, the well-known relation was used

$$\mu_A = \mu_{A_0}\frac{I_A}{I_{A_0}}\frac{a_A(nl)}{a_{A_0}(nl)}\left(1 + {}^{A_0}\Delta^A_{nl}\right), \tag{4}$$

where ${}^{A_0}\Delta^A_{nl}$ is the hyperfine structure anomaly (HFA) and n and l are the quantum numbers of the corresponding atomic state. The HFA arises from differences in charge and magnetization distribution within the nucleus through the "Breit-Rosenthal" (BR) [44] and "Bohr-Weisskopf" (BW) [45] effects, respectively. These effects are accounted for through parameters δ_A and ε_A,

$${}^{A_0}\Delta^A = {}^{A_0}\Delta^A_{\mathrm{BW}} + {}^{A_0}\Delta^A_{\mathrm{BR}} = (\varepsilon_{A_0} - \varepsilon_A) + (\delta_{A_0} - \delta_A).$$

In Ref. [35], the HFA for Tl isomers with $I = 9/2$ was determined experimentally,

$${}^{205}\Delta^A_{6P_{1/2}}(I = 9/2) = -0.007\,(2)\,. \tag{5}$$

This value has been used in the present paper for the magnetic-moment calculation for $^{185}\mathrm{Tl}^m$ ($I = 9/2$) by Eq. (4).

In Ref. [35], it was shown that the relativistic coupled-cluster approach [41] describes experimental data for the HFA in thallium fairly well. Therefore, this approach has been used in the present paper for the estimation of the HFA for other investigated Tl isotopes. In Ref. [34], the HFA for Tl isotopes was estimated by the application of the empirical Moskowitz-Lombardi rule [46]. However, recently it was shown [47] that this rule is not universal and should be applied to the HFA estimation with caution.

A. ^{183,185}Tl ($I = 1/2$)

In the framework of the model presented in Ref. [41], the HFA for Tl isotopes with $I = 1/2$ is determined mainly by the changes in the charge distribution parameter λ [see Eq. (3)] and similar magnetization distribution parameter,

$$\lambda_m = k_m(Z, I)\,\delta\langle r^2\rangle_m,$$

where $\langle r^2\rangle_m$ is the mean-square nuclear magnetization radius and k_m can be calculated by the formulas from Ref. [41]: $k_m(81,1/2) = 0.90$.

If one assumes $\delta\langle r^2\rangle_m = \delta\langle r^2\rangle$, then ${}^{205}\Delta^{183}_{6P_{1/2}}(I = 1/2) = -4.3 \times 10^{-4}$. However, from the comparison of the theoretical calculations with the experimental data for ${}^{205}\Delta^{203}_{6P_{1/2}}(I = 1/2)$, in Ref. [41], it was supposed that at least for this isotope pair, the change in the magnetic radius is more than twice as large as the change in the charge radius. By assuming that the ratio $\delta\langle r^2\rangle_m/\delta\langle r^2\rangle$ is constant for Tl isotopes with $I = 1/2$, one obtains ${}^{205}\Delta^{183}_{6P_{1/2}}(I = 1/2) = -8.0 \times 10^{-4}$.

By taking both limiting values of ${}^{205}\Delta^{183}_{6P_{1/2}}(I = 1/2)$ into account, the final estimation is ${}^{205}\Delta^{183}_{6P_{1/2}}(I = 1/2) = -6\,(4) \times 10^{-4}$. The similar estimations for $^{185}\mathrm{Tl}\,(I = 1/2)$ give the same value for the HFA.

B. ^{184}Tl^{m1} ($I = 2$)

For the odd-odd Tl isotopes with $I = 2$, the following possible configurations were considered: $(\pi s_{1/2},\nu f_{5/2})$, $(\pi s_{1/2},\nu p_{3/2})$, and $(\pi d_{3/2},\nu p_{1/2})$ [34]. A neutron configuration at the $f_{5/2}$ shell may be excluded for ^{184}Tl as it is expected to be at a much higher excitation energy in Tl isotopes close to the neutron midshell [22].

For odd-odd nuclei, the BW part of the HFA is related to the BW part of the HFA, generated by the unpaired proton (ε_π) and neutron (ε_ν) by

$$\varepsilon = \varepsilon_\pi\beta_\pi + \varepsilon_\nu\beta_\nu, \quad \beta_\pi = \frac{g_\pi}{g_I}\frac{g_I - g_\nu}{g_\pi - g_\nu}, \quad \beta_\nu = \frac{g_\nu}{g_I}\frac{g_I - g_\pi}{g_\nu - g_\pi}, \tag{6}$$

where g_π and g_ν are the single-particle g factors and β_π,β_ν are the fractional contributions of the proton and neutron to the total magnetic moment [48].

According to the additivity relation, the magnetic moment of a two-particle state $|i_p i_n I\rangle$ in the odd-odd nucleus may be calculated from

$$g_I = \frac{1}{2}(g_\pi + g_\nu) + \frac{1}{2}(g_\pi - g_\nu)\frac{i_p(i_p+1) - i_n(i_n+1)}{I(I+1)}, \tag{7}$$

where i_p and i_n are the proton and neutron single-particle angular moments.

To calculate the coefficients β_π,β_ν, one should know g_π and g_ν. These values can be determined from the known magnetic moments of the adjacent nuclei (as a rule, isotones and isotopes with the close Z and N, respectively). These values should, at the same time, match the experimental value of μ for the odd-odd nucleus in question by Eq. (7).

For the configuration $(\pi s_{1/2},\nu p_{3/2})$, g factors of ^{187}Tl [15] and ^{185}Pb [33] were used as g_π and g_ν. The magnetic moment of ^{184}Tl^{m1}, calculated by Eq. (7) ($\mu_{\rm th} = 0.42\mu_N$), is reasonably close to the experimental one [$\mu_{\rm exp} = 0.316(99)\mu_N$, see Table III]. To take the uncertainty in the g_ν factor into account, another value for it was also used (the g factor of ^{187}Hg [33]). By applying the formulas and constants from Refs. [35,41], the values of ε_π and ε_ν have been calculated. They give

$$^{205}\Delta^{184m}_{6P_{1/2}}[I = 2, (\pi s_{1/2}, \nu p_{3/2})] = -1.2(4) \times 10^{-3},$$

where the error reflects the possibility of the different choice of the $\delta\langle r^2\rangle_m/\delta\langle r^2\rangle$ ratio and g_ν.

A similar procedure for the configuration $(\pi d_{3/2},\nu p_{1/2})_2$ gives

$$^{205}\Delta^{184m}_{6P_{1/2}}[I = 2, (\pi d_{3/2}, \nu p_{1/2})] = -8\,(1) \times 10^{-3}.$$

As the magnetic moment of ^{184}Tl^{m1} is satisfactorily described by Eq. (7) for configuration $(\pi s_{1/2},\nu p_{3/2})_2$ with the g factors of adjacent Tl and Pb isotopes, the value of $^{205}\Delta^{184m}_{6P_{1/2}}$ for the pure $(\pi s_{1/2},\nu p_{3/2})$ configuration has been chosen as an estimation of the HFA. Nevertheless, the possibility of some admixture of the $(\pi d_{3/2},\nu p_{1/2})_2$ configuration cannot be excluded. Therefore, the uncertainty of the HFA was increased to take this presumable admixture into account: $^{205}\Delta^{184m}_{6P_{1/2}} = -1(7) \times 10^{-3}$. To elucidate this point, the measurements of $a(7s\,^2S_{1/2})$ and $a(6p\,^2P_{1/2})$ for Tl isotopes with $I = 2$ at an accuracy better than $\sim 1 \times 10^{-3}$ are desirable (see the procedure for extracting the HFA from the analysis of the hyperfine constants ratio, outlined in Ref. [35]).

C. ^{186}Tl^{m2} ($I = 10$)

The shell-model configuration for this isomer is supposed to be $(\pi h_{9/2},\nu i_{13/2})$ (see Ref. [22] and references therein).

With $\mu_\pi = \mu(^{187}\mathrm{Tl}^m, I = 9/2) = 3.707(22)\mu_N$ [35] and $\mu_\nu = \mu(^{185}\mathrm{Hg}^m, I = 13/2) = -1.017(9)\mu_N$ [2], one obtains $\mu_{\rm th}(^{186}\mathrm{Tl}^{m2}, I = 10) = 2.27(1)\mu_N$. The experimental value is rather close: $\mu_{\rm exp}(^{186}\mathrm{Tl}^{m2}, I = 10) = 2.55(6)\mu_N$ (see Table III). It is worth noting that, although the mean-square deformation of ^{187}Tl^m coincides with the mean-square deformation of ^{186}Tl^{m2} ($\langle\beta^2\rangle^{1/2} = 0.21$, see Fig. 4), the deformation of ^{185}Hg^m is markedly lower ($\langle\beta^2\rangle^{1/2} = 0.15$ [2]). During the recent IS and hfs measurements for the long chain of Po isotopes, it was shown that μ for the isotopes with $I = 13/2$ grows rather rapidly with the deformation increase [49]. Therefore, it is more reasonable to use in the HFA estimation the magnetic moment of ^{193}Po^m ($I = 13/2$) because this isotope practically has the same mean-square deformation as ^{186}Tl^{m2}, $\langle\beta^2\rangle^{1/2} = 0.22$ [49]. With $\mu_\nu = \mu(^{193}\mathrm{Po}^m, I = 13/2) = -0.74(6)\mu_N$ [49], the agreement of the calculated magnetic moment of the odd-odd Tl isotope with the experimental data is markedly improved: $\mu_{\rm th}(^{186}\mathrm{Tl}^{m2}, I = 10) = 2.53(12)\mu_N$. Both options for g_ν were used in the HFA estimation.

With the procedure outlined in the preceding section, one obtains

$$^{205}\Delta^{186m2}_{6P_{1/2}}[I = 10, (\pi h_{9/2}, \nu p_{13/2})] = -7.1(6) \times 10^{-3}.$$

Note that the calculated HFA proves to be rather great and coincides with the HFA for the odd Tl isomers with $I = 9/2$ [35]. This prediction can be checked by measuring $a(7s\,^2S_{1/2})$ and $a(6p\,^2P_{1/2})$ in ^{186}Tl^{m2} with an accuracy better than $\sim 2 \times 10^{-3}$.

In Table III, the magnetic moments of the Tl isotopes corrected by the estimated HFA as well as the uncorrected magnetic moments are presented. Only moments for the isotopes and isomers studied for the first time in the present paper and in our previous paper [35] are presented.

TABLE III. Magnetic moments of the thallium isotopes and isomers.

A	I	$\mu(\mu_N)$[a]	$\mu(\mu_N)$[b]
197m	9/2	4.062(57)	4.032(57)[c]
195m	9/2	3.898(38)	3.869(39)[c]
186m2	10	2.568(61)	2.549(62)
185g	1/2	1.608(38)	1.607(38)
185m	9/2	3.78(21)	3.75(21)
184m1	2	0.316(98)	0.316(99)
183g	1/2	1.619(37)	1.618(37)

[a]Without HFA correction.
[b]With HFA correction.
[c]Reference [35].

VI. DISCUSSION

A. Magnetic moments

In Fig. 3, the available data for the magnetic moments of different Tl nuclear states are presented. The newly measured magnetic moments follow the isotopic trend for the lighter or heavier nuclei with the same spin fairly well. This points to the smooth isotopic change in the nuclear structure of the Tl nuclei at the neutron midshell and beyond.

The intruder odd-odd isomer $^{186}\mathrm{Tl}^{m2}$ deserves special attention. Although the spin of this isomer is firmly established ($I = 10$, see Ref. [20]), other possible spin assignments ($I = 8,9$) have been checked. They lead to the noticeable discrepancy between the calculated ones by Eq. (7) and the measured magnetic moments. With the assumption $I = 8$, one obtains $\mu_{\mathrm{exp}}(^{186}\mathrm{Tl}^{m2}, I = 8) = 2.54(5)\mu_N$, whereas, $\mu_{\mathrm{th}}(^{186}\mathrm{Tl}^{m2}, I = 8) = 1.59\mu_N$ [with $\mu_\nu = \mu(^{193}\mathrm{Po}^m, I = 13/2) = -0.74\mu_N$] or $\mu_{\mathrm{th}}(^{186}\mathrm{Tl}^{m2}, I = 8) = 1.36\mu_N$ [with $\mu_\nu = \mu(^{185}\mathrm{Hg}^m, I = 13/2) = -1.017\mu_N$]. With the assumption $I = 9$, one obtains $\mu_{\mathrm{exp}}(^{186}\mathrm{Tl}^{m2}, I = 9) = 2.55(6)\mu_N$, whereas, $\mu_{\mathrm{th}}(^{186}\mathrm{Tl}^{m2}, I = 8) = 2.07\mu_N$ or $1.83\mu_N$ (with the same choices of μ_ν as above). At the same time, the assumption $I = 10$ leads to a good agreement between the measured and the calculated magnetic moments (see Sec. V C). This agreement may be regarded as an additional confirmation of the proposed intruder $(\pi h_{9/2}, \nu i_{13/2})_{10}$ configuration of this isomeric state.

B. Charge radii

In Fig. 4, changes in the mean-square charge radii $\delta\langle r^2\rangle_{A,205}$ of Tl nuclei are shown. It is generally acknowledged that the main isotopic trend of $\delta\langle r^2\rangle$ is described by the droplet model (DM) [50]. Deviations from the DM trend are attributed to the advance of the mean-square quadrupole deformation,

$$\langle r^2\rangle = \langle r^2\rangle_{\mathrm{DM}}\left(1 + \frac{5}{4\pi}\langle\beta^2\rangle\right).$$

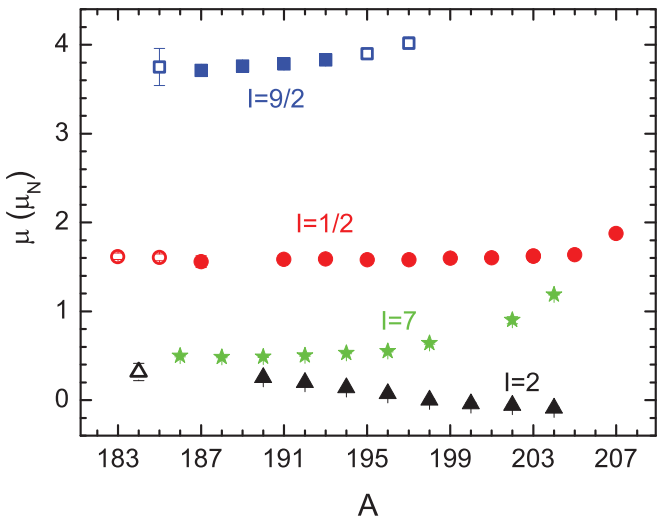

FIG. 3. (Color online) Magnetic moments for Tl isotopes and isomers. Squares: nuclei with $I = 9/2$; circles: nuclei with $I = 1/2$; triangles: nuclei with $I = 2$; asterisks: nuclei with $I = 7$. Full symbols: data from Refs. [7,10–18]; open symbols: present paper.

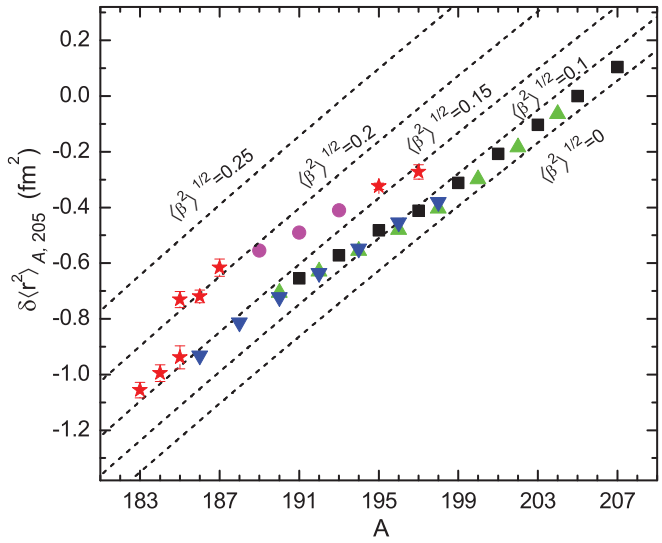

FIG. 4. (Color online) Isotopic dependency of the changes in the mean-square charge radii for Tl isotopes. Stars: present paper. Other values are recalculated from the IS data in Refs. [7–11,13,14,16–18], see Table II. Squares: nuclei with $I = 1/2$; circles: nuclei with $I = 9/2$; upward triangles: nuclei with $I = 2$; downward triangles: nuclei with $I = 7$. Dashed lines represent the droplet model prediction with different mean-square deformations. Droplet model predictions for $\delta\langle r^2\rangle_{A,205}$ are normalized by using $\langle\beta^2\rangle^{1/2}(^{205}\mathrm{Tl}) = 0.069$ (evaluated from $B(E2)$ for the core nucleus ^{204}Hg [51]). Only statistical errors are displayed. The possible change in the F or M factor would lead to the corresponding change in the y-axis scale and would not change the overall trend of the $\delta\langle r^2\rangle$ isotopic dependency.

In Fig. 4, the droplet model $\delta\langle r^2\rangle$ lines with a constant mean-square deformation are shown to get an insight into the development of the deformation in the Tl isotopic chain. In contrast to the mercury isotopic chain where strong odd-even staggering is present at $N < 105$ (see Ref. [2]), no strong odd-even staggering of the charge radii of the thallium isotope ground states is observed, and these states preserve their near-spherical shape even at the neutron midshell and beyond ($A < 186$). The similar smooth behavior of $\delta\langle r^2\rangle$, which testifies to the persistence of the near-spherical shape, was previously observed for Pb isotopes ($N = 100$–126) [4].

The rather great isomer shift between $I = 1/2$ and $I = 9/2$ states for odd Tl isotopes is preserved for both sides of the previously investigated mass range (i.e., for $A < 186$, $A > 192$). This means that the moderate oblate deformation is favored by the $h_{9/2}$ intruder state already in the comparable close vicinity of the neutron magic number $N = 126$ and it increases toward the midshell ($N = 104$). For the first time, a similar isomer jump in deformation is found for the odd-odd isotope ^{186}Tl. It is equal in the limits of errors to the isomer jump in deformation for the adjacent odd ^{185}Tl (see Fig. 4) with the isomeric state that stems from the $\pi h_{9/2}$ orbital.

In Ref. [5], deformations and excitation energies of the intrinsic states were calculated for a range of odd-mass thallium isotopes between $A = 181$ and 199 by using the shell correction method with the Woods-Saxon potential and a monopole pairing residual interaction. According to Ref. [5], the oblate deformation of the $9/2^-[505]$ state (identified with

the $9/2^-$ isomer) slowly decreases from -0.14 for ^{197}Tl to -0.16 for ^{185}Tl (cf. also the close results for ^{193,191,189}Tl^m in Ref. [52]). With nearly the same deformations, the rotational bands in the nuclei of ^{183,185,187}Tl were well described in the particle-triaxial-rotor model with a variable moment of inertia [53]. According to these calculations, the negative parity bands built upon the $9/2^-$ isomeric states in ^{183,185,187}Tl are formed by a proton with the $9/2^-[505]$ configuration coupled to a core with triaxial oblate deformation $(\beta,\gamma) = (-0.168,15^\circ)$, $(-0.164,15^\circ)$,$(-0.162,15^\circ)$, respectively. Note that the mean-square deformation, extracted from $\delta\langle r^2\rangle$ by the droplet model (see Fig. 4), shows a more pronounced change from 0.14 (^{197}Tl^m) to 0.21 (^{185}Tl^m). It should be noted that this conclusion is valid independent of the scaling F- and M-factor uncertainties. For example, the decrease in the F factor by 10% would give $\langle\beta^2\rangle^{1/2}(^{197}\text{Tl}^m) = 0.13$, $\langle\beta^2\rangle^{1/2}(^{185}\text{Tl}^m) = 0.20$. In Ref. [1], the mixing of two $9/2^-$ configurations in ^{183}Tl was assumed: One of them stems from the strongly prolate deformed band built on the low-Ω members of the $h_{9/2}$ shell, and the other is the bandhead of the moderately oblate deformed band, which coincides with the $9/2^-$ isomer [6]. A similar mixture may also be expected in ^{185}Tl as the corresponding $9/2^-$ states are still situated not far from each other: The energy difference $\delta E(9/2^-_{\text{prol}} - 9/2^-_{\text{obl}})$ between the two $9/2^-$ states from the oblate and prolate $h_{9/2}$ bands in ^{185}Tl is equal to 316 keV (see Ref. [19]); compare with $\delta E(9/2^-_{\text{prol}} - 9/2^-_{\text{obl}}) = 299$ keV for ^{183}Tl (see Ref. [6]). If this mixture really takes place, the mean-square deformation of the $9/2^-$ isomer would increase as the absolute value of the deformation of the prolate deformed $h_{9/2}$ states is markedly greater than that of the oblate deformed $h_{9/2}$ states (up to $\beta = 0.24$ for the $3/2^-[532]h_{9/2}$ band; see Refs. [5,53]). Thus, this mixture may explain the increase in the mean-square deformation for the $9/2^-$ isomer in comparison with the calculations. It would be desirable to measure the isomer shift for ^{183}Tl where the presumed mixture (and, correspondingly, the mean-square deformation and isomer shift) should be greater than for ^{185}Tl.

The similarities between the different isotopic chains in the lead region can be elucidated by comparing relative changes in the mean-square charge radii $\delta\langle r^2\rangle$ [54]. The values of $\delta\langle r^2\rangle_{N,126}$ are normalized within each isotopic chain to $\delta\langle r^2\rangle_{122,124}$ to allow for a comparison between these chains. Figures 5 and 6 show the relative changes in $\delta\langle r^2\rangle$ for the lead and thallium nuclei. For Pb nuclei, the IS data from Refs. [4,36] were used. Values of the relative changes in $\delta\langle r^2\rangle$ are independent of an electronic factor F, although they may be changed with the different choices of a mass shift constant M. For Pb nuclei, the same condition ($M_{\text{SMS}} = 0$) as was set for the similar atomic transition in Tl was chosen. This choice does not contradict with the assumptions used previously: $M_{\text{SMS}} = 0.19(25) \times M_{\text{NMS}}$ [4], $M_{\text{SMS}} = 8(10) \times M_{\text{NMS}}$ [36].

For the sake of clarity, results for the even-neutron and odd-neutron nuclei are presented in the different figures (Fig. 5 for the even-neutron nuclei and Fig. 6 for the odd-neutron nuclei). For odd-neutron nuclei, the data for ground states with the odd neutron on the same shell ($\nu p_{3/2}$) are displayed. It is clearly seen that the Tl radii perfectly follow the pattern of the Pb radii

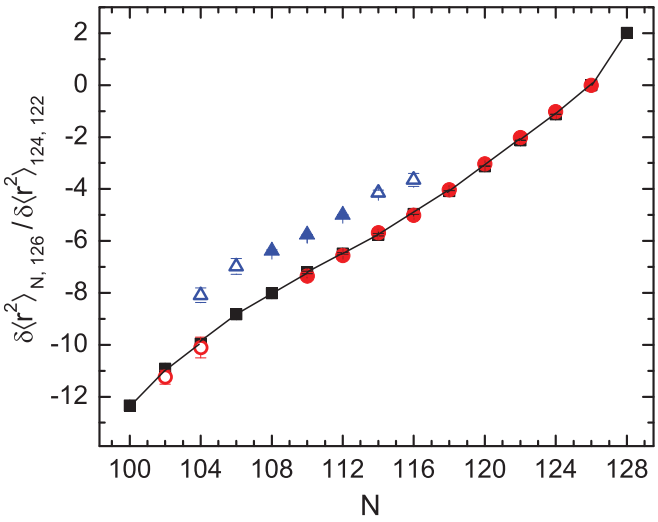

FIG. 5. (Color online) Relative changes in $\delta\langle r^2\rangle$ for the even-neutron lead and thallium isotopes. Boxes connected by the line (to guide the eye) represent the values for even Pb isotopes (the IS data are taken from Refs. [4,36]). Circles represent the values for odd Tl ground states with $I = 1/2$ (see Table II and references therein). Triangles represent the values for odd Tl isomers with $I = 9/2$ (see Table II and references therein). Open symbols show the values obtained in the present paper.

even below the midshell at $N = 104$ where the well-known pronounced deviation from this behavior, connected with the onset of permanent prolate deformation, was found for the adjacent Hg ($Z = 80$, Ref. [2]) and Au ($Z = 79$, Ref. [3]) nuclei.

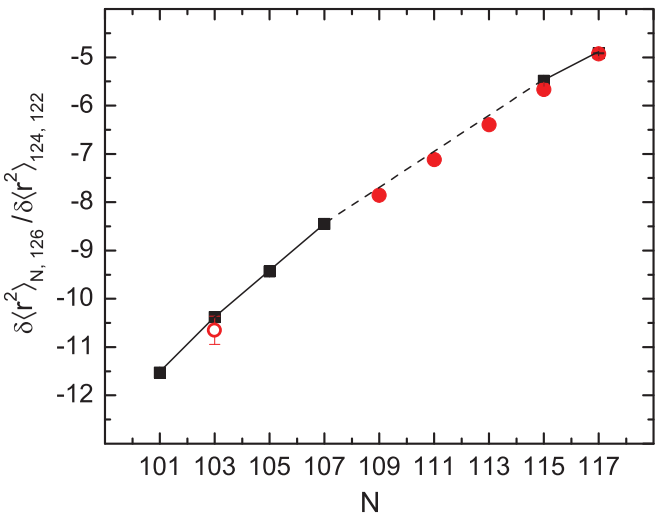

FIG. 6. (Color online) Relative changes in $\delta\langle r^2\rangle$ for the odd-neutron lead and thallium isotopes. Boxes connected by the line (to guide the eye) represent the values for odd Pb isotopes with $I = 3/2$ (the IS data are taken from Refs. [4,36]). Circles represent the values for even Tl ground states with $I = 2$ (see Table II and references therein). The open symbol shows the value obtained in the present paper.

VII. CONCLUSIONS

Hyperfine structures and isotope shifts in the 276.9-nm atomic transition in a long chain of thallium isotopes and isomers have been studied. From the comparison with the previously measured ISs of the 535-nm transition for $^{186-194,203,205}$Tl, the electronic parameters needed for extraction of the $\delta\langle r^2\rangle$ from the IS data for the 276.9-nm transition have been determined. New data on the magnetic moments and $\delta\langle r^2\rangle$ for ^{183,185}Tl and ^{184,186,195,197}Tl^m have been obtained. It has been shown that nuclear properties for Tl isotopes and isomers smoothly change at the neutron midshell and beyond. The rather great isomer shift between $I = 1/2$ and $I = 9/2$ states for odd Tl isotopes is preserved for both sides of the previously investigated mass range. For the first time, a similar isomer shift is found for the odd-odd isotope ^{186}Tl. The close resemblance of the charge radii isotopic behavior for the Tl and Pb ground states down to $N = 102$ is demonstrated.

[1] K. Heyde and J. L. Wood, Rev. Mod. Phys. **83**, 1467 (2011).

[2] G. Ulm, S. K. Bhattacherjee, P. Dabkiewicz, G. Huber, H.-J. Kluge, T. Kühl, H. Lochmann, E.-W. Otten, K. Wendt, S. A. Ahmad, W. Klempt, R. Neugart, and the ISOLDE Collaboration, Z. Phys. A **325**, 247 (1986).

[3] K. Wallmeroth, G. Bollen, A. Dohn, P. Egelhof, U. Kronert, M. J. G. Borge, J. Campos, A. Rodriguez Yunta, K. Heyde, C. De Coster, L. Wood, H.-J. Kluge, and the ISOLDE Collaboration, Nucl. Phys. A **493**, 224 (1989).

[4] M. D. Seliverstov, A. N. Andreyev, N. Barré, A. E. Barzakh, S. Dean, H. De Witte, D. V. Fedorov, V. N. Fedoseyev, L. M. Fraile, S. Franchoo, J. Genevey, G. Huber, M. Huyse, U. Köster, P. Kunz, S. R. Lesher, B. A. Marsh, I. Mukha, B. Roussière, J. Sauvage, I. Stefanescu, K. Van de Vel, P. Van Duppen, and Y. M. Volkov, Eur. Phys. J. A **41**, 315 (2009).

[5] G. J. Lane, G. D. Dracoulis, A. P. Byrne, P. M. Walker, A. M. Baxter, J. A. Sheikh, and W. Nazarewicz, Nucl. Phys. A **586**, 316 (1995).

[6] P. M. Raddon, D. G. Jenkins, C. D. O'Leary, A. J. Simons, R. Wadsworth, A. N. Andreyev, R. D. Page, M. P. Carpenter, F. G. Kondev, T. Enqvist, P. T. Greenlees, P. M. Jones, R. Julin, S. Juutinen, H. Kettunen, M. Leino, A.-P. Leppänen, P. Nieminen, J. Pakarinen, P. Rahkila, J. Uusitalo, and D. T. Joss, Phys. Rev. C **70**, 064308 (2004).

[7] R. Menges, U. Dinger, N. Boos, G. Huber, S. Schroder, S. Dutta, R. Kirchner, O. Klepper, T. Kühl, D. Marx, and G. D. Sprouse, Z. Phys. A **341**, 475 (1992).

[8] G. Hermann, G. Lasnitschka, and D. Spengler, Z. Phys. D **28**, 127 (1993).

[9] W. Lauth, H. Backe, M. Dahlinger, I. Klaft, P. Schwamb, G. Schwickert, N. Trautmann, and U. Othmer, Phys. Rev. Lett. **68**, 1675 (1992).

[10] R. Neugart, H. H. Stroke, S. A. Ahmad, H. T. Duong, H. L. Ravn, and K. Wendt, Phys. Rev. Lett. **55**, 1559 (1985).

[11] R. J. Hull and H. H. Stroke, J. Opt. Soc. Am. **51**, 1203 (1961).

[12] D. S. Richardson, R. N. Lyman, and P. K. Majumder, Phys. Rev. A **62**, 012510 (2000).

[13] H. A. Schuessler, E. C. Benck, F. Buchinger, and H. K. Carter, Nucl. Instrum. Methods Phys. Res. A **352**, 583 (1995).

[14] J. A. Bounds, C. R. Bingham, H. K. Carter, G. A. Leander, R. L. Mlekodaj, E. H. Spejewski, and W. M. Fairbank Jr., Phys. Rev. C **36**, 2560 (1987).

[15] H. A. Schuessler, E. C. Benck, F. Buchinger, H. Iimura, Y. F. Li, C. Bingham, and H. K. Carter, Hyperfine Interact. **74**, 13 (1992).

[16] D. Goorvitch, H. Kleiman, and S. P. Daviset, Nucl. Phys. A **99**, 1 (1967).

[17] S. P. Davis, H. Kleiman, D. Goorvitch, and T. Aung, J. Opt. Soc. Am. **56**, 1604 (1966).

[18] D. Goorvitch, S. P. Davis, and H. Kleiman, Phys. Rev. **188**, 1897 (1969).

[19] http://www.nndc.bnl.gov/ensdf/

[20] A. J. Kreiner, C. Baktash, G. Garcia Bermudez, and M. A. J. Mariscotti, Phys. Rev. Lett. **47**, 1709 (1981).

[21] P. Van Duppen, P. Decrock, P. Dendooven, M. Huyse, G. Reusen, and J. Wauters, Nucl. Phys. A **529**, 268 (1991).

[22] A. N. Andreyev, D. Ackermann, S. Antalic, H. J. Boardman, P. Cagarda, J. Gerl, F. P. Heßberger, S. Hofmann, M. Huyse, D. Karlgren, A. Keenan, H. Kettunen, A. Kleinböhl, B. Kindler, I. Kojouharov, A. Lavrentiev, C. D. O'Leary, M. Leino, B. Lommel, M. Matos, C. J. Moore, G. Münzenberg, R. D. Page, S. Reshitko, S. Saro, H. Schaffner, C. Schlegel, M. J. Taylor, K. Van de Vel, P. Van Duppen, L. Weissman, and K. Heyde, Eur. Phys. J. A **18**, 39 (2003).

[23] G. D. Alkhazov, A. E. Barzakh, V. P. Denisov, K. A. Mezilev, Y. N. Novikov, V. N. Panteleyev, A. V. Popov, E. P. Sudentas, V. S. Letokhov, V. I. Mishin, V. N. Fedoseyev, S. V. Andreyev, D. S. Vedeneyev, and A. D. Zyuzikov, Nucl. Instrum. Methods Phys. Res. B **69**, 517 (1992).

[24] A. E. Barzakh, I. Y. Chubukov, D. V. Fedorov, V. N. Panteleev, M. D. Seliverstov, and Y. M. Volkov, Phys. Rev. C **61**, 034304 (2000).

[25] V. N. Fedosseev, D. V. Fedorov, R. Horn, G. Huber, U. Köster, J. Lassen, V. I. Mishin, M. D. Seliverstov, L. Weissman, K. Wendt, and the ISOLDE Collaboration, Nucl. Instrum. Methods Phys. Res. B **204**, 353 (2003).

[26] A. E. Barzakh, D. V. Fedorov, V. S. Ivanov, P. L. Molkanov, V. N. Panteleev, and Y. M. Volkov, Rev. Sci. Instrum. **83**, 02B306 (2012).

[27] V. N. Panteleev, O. Alyakrinskiy, M. Barbui, A. E. Barzakh, D. V. Fedorov, V. S. Ivanov, G. Lhersonneau, K. A. Mezilev, P. L. Molkanov, F. V. Moroz, S. Y. Orlov, L. Stroe, L. B. Tecchio, M. Tonezzer, and Y. M. Volkov, Eur. Phys. J. A **42**, 495 (2009).

[28] A. Lurio and A. G. Prodel, Phys. Rev. **101**, 79 (1956).

[29] H. Kopfermann, *Nuclear Moments* (Academic, New York, 1958).

[30] K.-H. Weber, J. Lawrenz, A. Obrebski, and K. Niemax, Phys. Scr. **35**, 309 (1987).

[31] S. J. Rehse, W. M. Fairbank Jr., and S. Au Lee, J. Opt. Soc. Am. B **18**, 855 (2001).

[32] M. Brieger, H. Bucka, A. Reichelt, and P. Zimmermann, Z. Naturforsch., A: Astrophys., Phys. Phys. Chem. **24**, 903 (1969).

[33] N. J. Stone, At. Data Nucl. Data Tables **90**, 75 (2005).

[34] C. Ekström, G. Wannberg, and Y. S. Shishodia, Hyperfine Interact. **1**, 437 (1975).

[35] A. E. Barzakh, L. K. Batist, D. V. Fedorov, V. S. Ivanov, K. A. Mezilev, P. L. Molkanov, F. V. Moroz, S. Y. Orlov, V. N. Panteleev, and Y. M. Volkov, Phys. Rev. C **86**, 014311 (2012).

[36] G. Fricke and K. Heilig, *Nuclear Charge Radii* (Springer, Berlin, 2004).
[37] G. Torbohm, B. Fricke, and A. Rosén, Phys. Rev. A **31**, 2038 (1985).
[38] B. Fricke (private communication cited in Ref. [8]).
[39] B. Fricke (private communication cited in Ref. [7]).
[40] A. C. Hartley and A.-M. Mårtensson-Pendrill, J. Phys. B **24**, 1193 (1991); A. C. Hartley, A.-M. Mårtensson-Pendrill, and A. Ynnerman (private communication cited in Ref. [7]).
[41] A.-M. Mårtensson-Pendrill, Phys. Rev. Lett. **74**, 2184 (1995).
[42] H. A. Schuessler, E. C. Benck, F. Buchinger, R. Wyss, C. R. Bingham, H. K. Carter, and J. Rikovska-Stone, Abstracts of the 6th Intern. Conference on Nuclei Far from Stability + 9th International Conference on Atomic Masses and Fundamental Constants, Bernkastel-Kues, Germany, 19–24 July 1992 (unpublished).
[43] E. W. Otten, in *Treatise on Heavy-Ion Science*, edited by D. A. Bromley (Plenum, New York, 1989), Vol. 8, p. 517.
[44] J. E. Rosenthal and G. Breit, Phys. Rev. **41**, 459 (1932).
[45] A. Bohr and V. F. Weisskopf, Phys. Rev. **77**, 94 (1950).
[46] P. A. Moskowitz and M. Lombardi, Phys. Lett. B **46**, 334 (1973).
[47] J. R. Persson, Hyperfine Interact. **162**, 139 (2005).
[48] C. Ekström, L. Robertsson, S. Ingelman, G. Wannberg, and I. Ragnarsson, Nucl. Phys. A **348**, 25 (1980).
[49] M. D. Seliverstov, T. E. Cocolios, W. Dexters, A. N. Andreyev, S. Antalic, A. E. Barzakh, B. Bastin, J. Büscher, I. G. Darby, D. V. Fedorov, V. N. Fedoseyev, K. T. Flanagan, S. Franchoo, S. Fritzsche, G. Huber, M. Huyse, M. Keupers, U. Köster, Y. Kudryavtsev, B. A. Marsh, P. L. Molkanov, R. D. Page, A. M. Sjødin, I. Stefan, J. Van de Walle, P. Van Duppen, M. Venhart, and S. G. Zemlyanoy, Phys. Lett. B **719**, 362 (2013); M. D. Seliverstov (private communication).
[50] D. Berdichevsky and F. Tondeur, Z. Phys. A **322**, 141 (1985).
[51] S. Raman, C. W. Nestor Jr., and P. Tikkanen, At. Data Nucl. Data Tables **78**, 1 (2001).
[52] J. A. Bounds, C. R. Bingham, P. Juncar, H. K. Carter, G. A. Leander, R. L. Mlekodaj, E. H. Spejewski, and W. M. Fairbank Jr., Phys. Rev. Lett. **55**, 2269 (1985).
[53] G.-j. Chen, Y.-x. Liu, H.-c. Song, and H. Cao, Phys. Rev. C **73**, 034304 (2006).
[54] R. J. Hull and H. H. Stroke, Phys. Rev. **122**, 1574 (1961).